

Coordinated Assembly of Galaxy Groups and Clusters in the IllustrisTNG Simulations

MENG GU¹, CHARLIE CONROY², BENEDIKT DIEMER³, LARS HERNQUIST², FEDERICO MARINACCI⁴, DYLAN NELSON⁵, RÜDIGER PAKMOR⁵, ANNALISA PILLEPICH⁶, MARK VOGELSBERGER⁷

Submitted to ApJL

ABSTRACT

Recent stellar population analysis of early-type galaxy spectra has demonstrated that the low-mass galaxies in cluster centers have high $[\alpha/\text{Fe}]$ and old ages characteristic of massive galaxies and *unlike* the low-mass galaxy population in the outskirts of clusters and fields. This phenomenon has been termed “coordinated assembly” to highlight the fact that the building blocks of massive cluster central galaxies are drawn from a special subset of the overall low-mass galaxy population. Here we explore this idea in the IllustrisTNG simulations, particularly the TNG300 run, in order to understand how environment, especially cluster centers, shape the star formation histories of quiescent satellite galaxies in groups and clusters ($M_{200c, z=0} \geq 10^{13} M_{\odot}$). Tracing histories of quenched satellite galaxies with $M_{*, z=0} \geq 10^{10} M_{\odot}$, we find that those in more massive dark matter halos, and located closer to the primary galaxies, are quenched earlier, have shorter star formation timescales, and older stellar ages. The star formation timescale- M_{*} and stellar age- M_{*} scaling relations are in good agreement with observations, and are predicted to vary with halo mass and cluster-centric distance. The dependence on environment arises due to the infall histories of satellite galaxies: galaxies that are located closer to cluster centers in more massive dark matter halos at $z=0$ were accreted earlier on average. The delay between infall and quenching time is shorter for galaxies in more massive halos, and depends on the halo mass at its first accretion, showing that group pre-processing is a crucial aspect in satellite quenching.

Keywords: methods: numerical — galaxies: clusters: general — galaxies: groups: general — galaxies: formation — galaxies: evolution — galaxies: halos

1. INTRODUCTION

Recent observations and simulations provide us an increasingly clear picture of the build-up of massive early type galaxies (ETGs) (Naab et al. 2009; Oser et al. 2010, 2012; van Dokkum et al. 2010; Patel et al. 2013). At high- z , strong dissipational processes such as gas accretion and gas rich mergers lead to rapid star formation, while at lower redshifts the accretion of low-mass systems dominate their growth. The disrupted low-mass galaxies are predicted to leave their imprint, such as stellar population information, on massive galaxies, especially in their outer envelopes (Di Matteo et al. 2009; Cook et al. 2016). Meanwhile, observations of nearby ETGs reveal scaling relations between their stellar mass and stellar populations, e.g., stellar metallicity, stellar age, α -abundance (Trager et al. 2000; Thomas et al. 2005; Conroy et al. 2014). Whether the building blocks of massive galaxies are intrinsically the same as the low-mass galaxies we observe today is still in debate.

In a recent paper, Gu et al. (2018), we described the “Coordinated Assembly” picture of massive galaxies using observations of an ongoing brightest cluster galaxy (BCG) assembly

in Abell 3827. We found that the ETGs in the central regions of the galaxy cluster do not follow the $[\alpha/\text{Fe}]-M_{*}$ and age- M_{*} trends established by the general ETG sample, but instead obey much shallower relations. Our work indicates that the building blocks of massive galaxies in this special environment are different from the overall ETG population. As a result, massive central galaxies grow by accreting preferentially high $[\alpha/\text{Fe}]$ and old stellar systems. The flat age and $[\alpha/\text{Fe}]$ radial profiles confirm that the disrupted systems should be old and α -enhanced.

This picture highlights the role that environment has on galaxy quenching (Peng et al. 2010; Peng et al. 2012; Wetzel et al. 2013, 2014): ETGs in the central region of galaxy clusters have ceased their star formation activity earlier than their counterparts elsewhere. Galaxy quenching could be due to multiple physical mechanisms, including strangulation (Larson et al. 1980; Balogh et al. 2000), ram-pressure stripping (Gunn & Gott 1972; Abadi et al. 1999), harassment (Farouki & Shapiro 1981; Moore et al. 1996), etc. These processes preferentially occur when a galaxy falls into a high density environment, but the details about how these mechanisms depend on environment, e.g., halo mass or local over-density, is still ambiguous.

Comparing observations with cosmological hydrodynamical simulations grants us access to a more complete history about how those galaxies form in different environments, and allows us to explore the coordinated assembly picture in detail. The IllustrisTNG suites are state-of-the-art hydrodynamical simulations that include a large population of massive galaxy clusters (Springel et al. 2018; Pillepich et al. 2018; Pillepich et al. 2019; Naiman et al. 2018; Marinacci et al. 2018; Nelson et al. 2018; Nelson et al. 2019b,a), and allows us to trace the life stories of a statistical sample of massive galaxies and their surrounding satellite galaxies

¹ Department of Astrophysical Sciences, Princeton University, Princeton, NJ 08544, USA

² Department of Astronomy, Harvard University, Cambridge, MA 02138, USA

³ Department of Astronomy, The University of Maryland, College Park, MD 20742

⁴ Department of Physics and Astronomy, University of Bologna, Via Gobetti 93/2, I-40129, Bologna, Italy

⁵ Max-Planck-Institut für Astrophysik, Karl-Schwarzschild-Str. 1, D-85748, Garching, Germany

⁶ Max-Planck-Institut für Astronomie, Königstuhl 17, D-69117 Heidelberg, Germany

⁷ Department of Physics, Massachusetts Institute of Technology, Cambridge, MA 02139

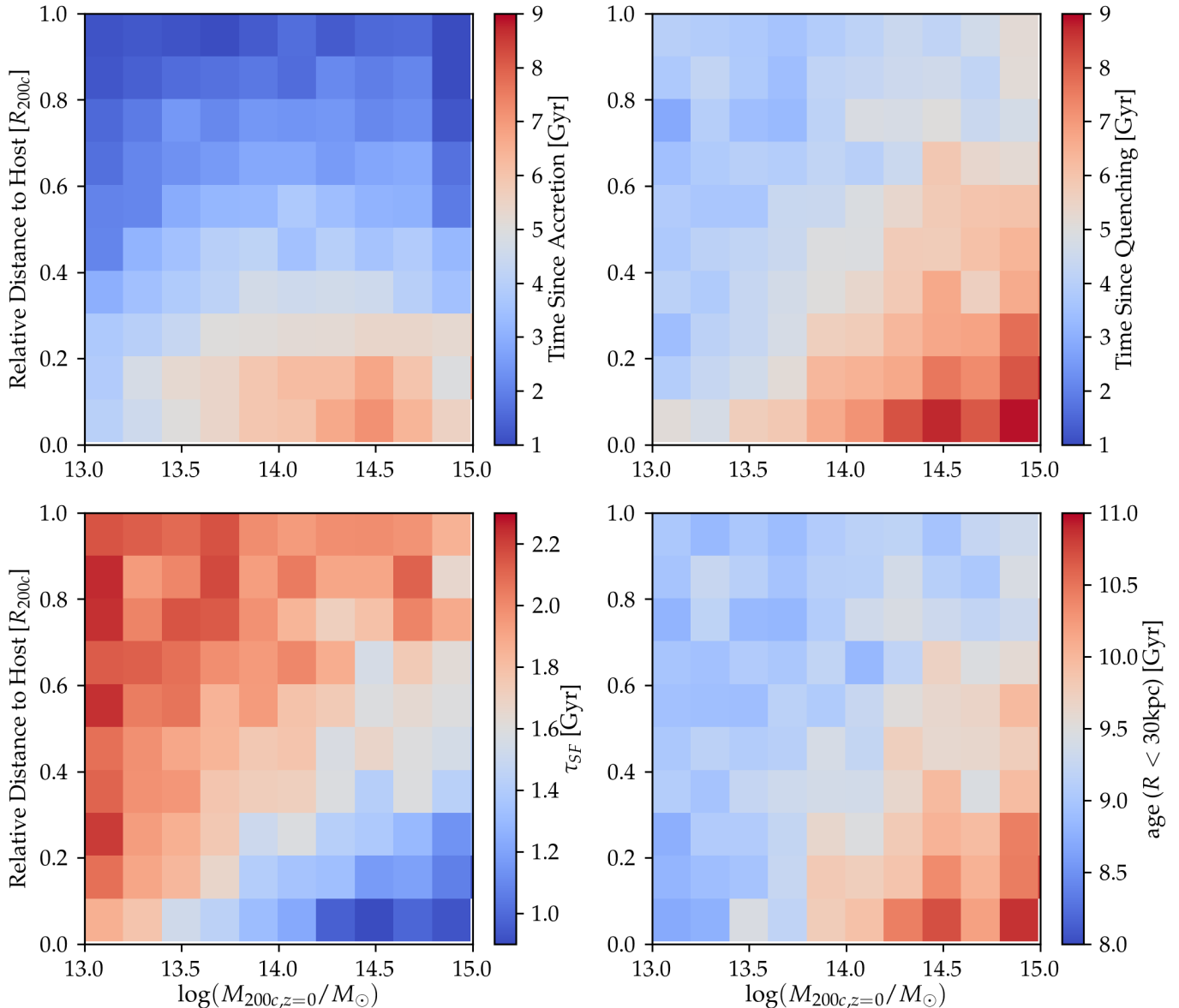


Figure 1. Variation of parameters for TNG300 quiescent satellite galaxies with $10 \leq \log(M_{*,z=0}/M_{\odot}) < 11$ at $z=0$ in the plane of host halo mass at $z=0$ and their relative 3D distance to the primary galaxies. From top left to bottom right, the parameters are the time since galaxies accreted to the R_{200c} of their final host dark matter halo, the time since galaxies are quenched, the star formation timescales, and the mass-weighted stellar age within 30 kpc. Colors indicate the mean values in the bins of $0.1R_{200c}$ and 0.2 dex in cluster-centric distance and halo mass directions, respectively. The minimum number of galaxies in any bin is 29.

in groups and clusters. In this paper, we focus on quenched satellite galaxies. The contribution from star forming satellite galaxies, although they may be the minority in clusters, also depends on environment (Donnari et al. 2020). By directly analyzing the star formation, quenching, and assembly histories of ETGs in IllustrisTNG, we address the following questions: Does the coordinated assembly picture hold in IllustrisTNG? Are the relevant scaling relations consistent with observations? What is the possible explanation for the coordinated assembly picture?

In this Letter, we briefly review how we make use of the simulations in Section 2, and present the results, including the environmental dependence, and comparison with observations in Section 3. We discuss the importance of group pre-processing as well before summarizing our conclusions in Section 4.

2. METHODS

The IllustrisTNG suite is a set of cosmological gravito-magneto-hydrodynamical simulations (Springel et al. 2018; Pillepich et al. 2018; Pillepich et al. 2019; Naiman et al. 2018; Marinacci et al. 2018; Nelson et al. 2018; Nelson et al. 2019b,a), based on the original Illustris simulations (Genel et al. 2014; Vogelsberger et al. 2014a,b). Significant improvements in the galaxy formation model provide a more realistic prediction of galaxy evolution. The galaxies are more consistent with observations in terms of galaxy sizes and morphological types, star formation stellar contents, etc (e.g. Pillepich et al. 2018; Nelson et al. 2018; Genel et al. 2018; Rodriguez-Gomez et al. 2019; Diemer et al. 2017; Donnari et al. 2019). The IllustrisTNG simulations adopt the Λ CDM cosmology with parameters from Planck Collaboration et al. (2016): $h=0.6774$, $\Omega_{m,0}=0.3089$, $\Omega_{b,0}=0.0486$, $\sigma_8=0.8159$, and $n_s=0.9667$. It includes three different cosmological vol-

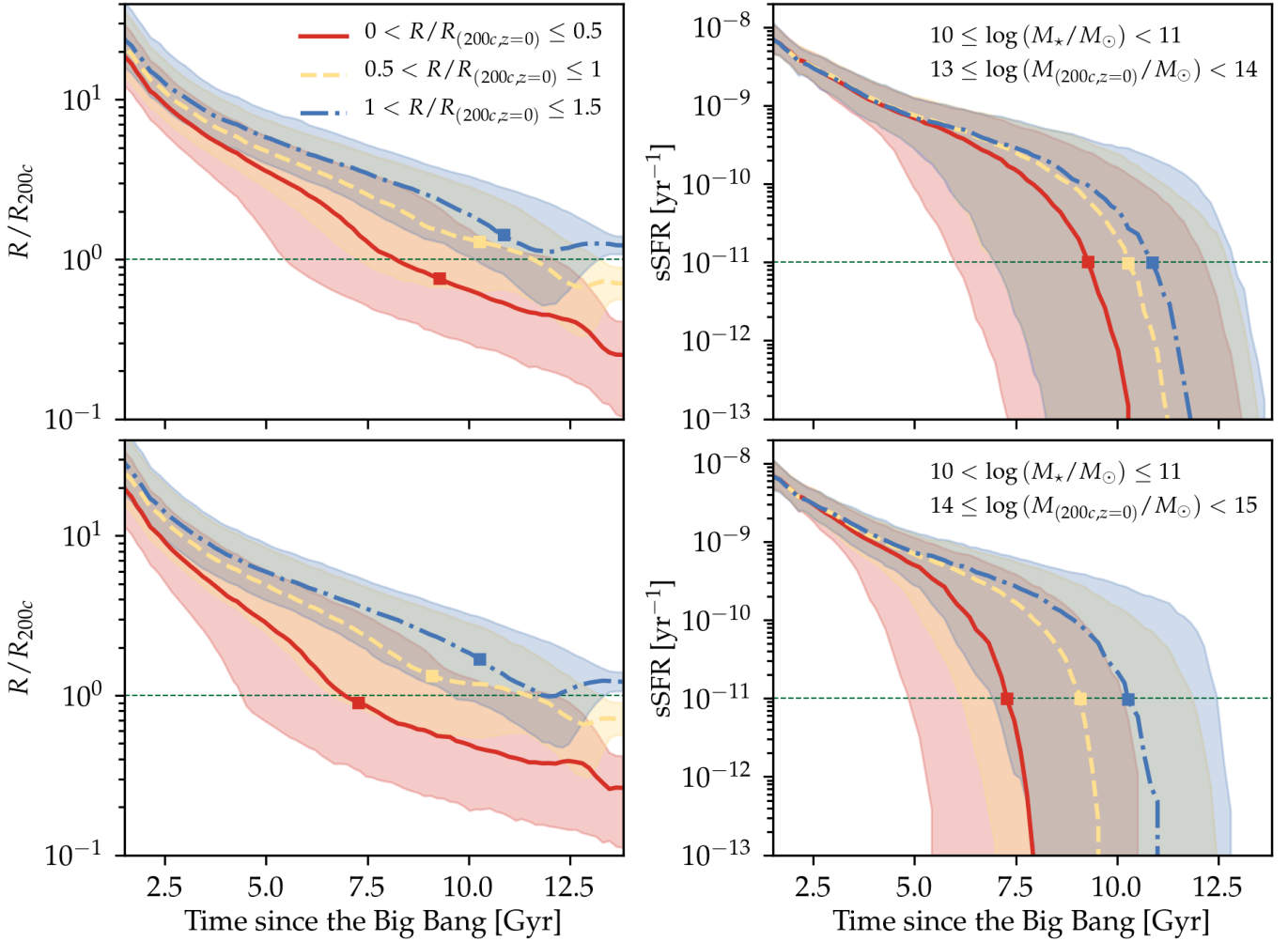


Figure 2. Evolution of TNG300 quiescent satellite galaxies selected at $z=0$ with $10 \leq \log(M_{*,z=0}/M_{\odot}) < 11$ in two halo mass bins, $13 \leq \log(M_{200c,z=0}/M_{\odot}) < 14$ (top panels) and $14 \leq \log(M_{200c,z=0}/M_{\odot}) < 15$ (bottom panels). Left panels show the evolution of their distances relative to the final primary galaxies at $z=0$, grouped by their relative distances at $z=0$. Right panels show the evolution of sSFR in each relative distance group. Lines and shaded regions indicate median and $\pm 1\sigma$ values. Squares mark the time that satellite galaxies are quenched. In both massive clusters and groups, satellite galaxies closer to the halo centers, and in more massive dark matter halos at $z=0$ have earlier accretion histories and quenching histories.

umes. In this Letter, we focus on the TNG300 run, the run of the IllustrisTNG simulations with the largest box with a side length of about 300 Mpc. The mass resolution of the TNG300 simulation is $5.9 \times 10^7 M_{\odot}$ for dark matter and $1.1 \times 10^7 M_{\odot}$ for baryons. The combination between the simulated volume and resolution makes this run an ideal one for studying the formation and assembly histories of the massive galaxies and their satellites in clusters.

We make use of the halos and subhalos identified by the friends-of-friends (FOF) (Davis et al. 1985) and SUBFIND (Springel et al. 2001; Dolag et al. 2009) algorithms, and merger trees generated by the SUBLINK algorithm (Rodríguez-Gomez et al. 2015). Throughout this work, we focus on groups and clusters with $M_{200c} \geq 10^{13} M_{\odot}$. There are 3733 such dark matter halos at $z=0$ up to a cluster of $\sim 10^{15} M_{\odot}$, each modeled with dark matter, gas, stars, magnetic fields and SMBHs. The stellar mass of a galaxy refers to the total stellar mass of all stellar particles within 30 kpc. We employ only the well-resolved galaxies so the minimum stellar mass in our sample is $10^{10} M_{\odot}$. We focus on quiescent galaxies in this work, and select galaxies with a specific star-formation rate (sSFR) less than 10^{-11}yr^{-1} at

$z=0$, and only satellite galaxies, excluding primary galaxies in our sample. The satellite galaxies in this work are all those within parent FOF groups above the mass threshold, including those located outside R_{200c} . There are 615, 8914 and 19389 quiescent satellite galaxies with $M_{*} \geq 10^{10} M_{\odot}$ in halos with M_{200c} more than $10^{15} M_{\odot}$, $10^{14} M_{\odot}$ and $10^{13} M_{\odot}$, respectively. We calculate the quenching time, star formation timescale, and the accretion time by tracing the main progenitors of galaxies selected at $z=0$ back in time. Specifically, we calculate the time since quenching as the time since a galaxy’s sSFR last fell and remained below $10^{-11}/\text{yr}$. We define the time since accretion as the time since a satellite galaxy initially fell within R_{200c} of its host dark matter halo. The star formation timescale is calculated using stars formed in-situ, as in Rodríguez-Gomez et al. (2016). The star formation timescale refers to half of the time it takes for the galaxy to form between 16% and 84% of its in-situ stars. The stellar ages in this work refer to the mass-weighted stellar ages within 30 kpc from the galaxy center.

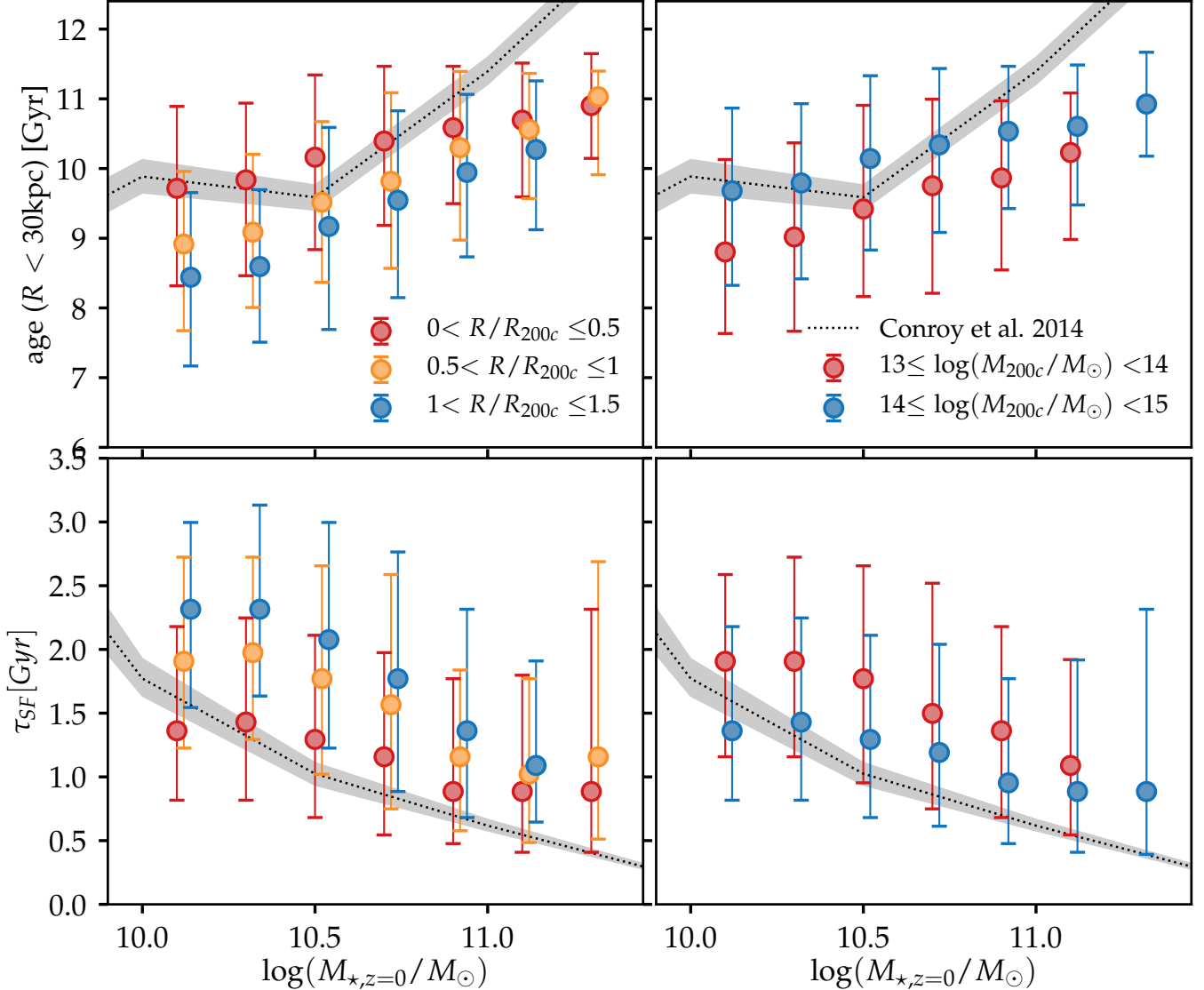


Figure 3. Scaling relations between stellar mass and stellar ages (top panels), and star formation timescales (τ_{SF} , bottom panels) for satellite galaxies in the TNG300 simulation. Galaxies are grouped by their relative distance to the primary galaxies in the dark matter halos with $M_{200c} \geq 10^{14} M_{\odot}$ at $z = 0$ (left panels), or the mass of their final host dark matter halos (right panels). Colored points indicate the median values and error-bars enclose the 25th and 75th percentiles of the simulation results. Observational results are shown in black and gray and are measured from the stacked spectra of SDSS ETGs in all environments (Conroy et al. 2014).

3. RESULTS AND DISCUSSION

3.1. Dependence on Halo Mass and Cluster-centric Distance

Figure 1 shows the coordinated assembly signal in the TNG300 simulation. Specifically, the panels show the dependence on environment. We focus on quenched satellite galaxies in a small stellar mass range at $z = 0$, $10 \leq \log(M_{*,z=0}/M_{\odot}) < 11$, and show their accretion time (top left), their quenching time (top right), the star formation timescale (bottom left) and their mass-weighted stellar age (bottom right) in this figure. The color-maps show the mean values of these parameters as a function of both the 3D cluster-centric distance at $z = 0$ in $0.1R_{200c}$ bins, and their host halo mass (M_{200c}) in 0.2 dex bins. The figure reveals a strong dependence on environment for all four parameters. From the top two panels, in general, quenched satellite galaxies that live in more massive halos and are located closer to the cen-

tral galaxies are accreted to R_{200c} earlier and quenched earlier, possibly because an early accretion means they may get the chance to experience all the quenching mechanisms earlier and/or longer than their counterparts. In fact, as shown in Rhee et al. (2017), satellites at small cluster-centric distances have accreted earlier. Those located at $\leq 0.2 \times R_{200c}$ in massive clusters ($M_{200c,z=0} \geq 10^{14} M_{\odot}$) at $z = 0$ are accreted $\sim 7-8$ Gyr ago and quenched $\sim 6-8$ Gyr ago, while those at $\sim R_{200c}$ in low mass dark matter halos ($10^{13} M_{\odot} \leq M_{200c,z=0} < 10^{14} M_{\odot}$) are only accreted and quenched $\sim 3-4$ Gyr ago. Looking at the most massive bins with the smallest cluster-centric distance, the trend of time since accretion does not peak in the most massive halo mass bin. There are several reasons for this: 1. the fraction of pre-processed galaxies (which will be discussed in Section 3.3) increases with increasing mass of the final host halos. 2. On average, satellite galaxies that have been pre-processed are accreted into the

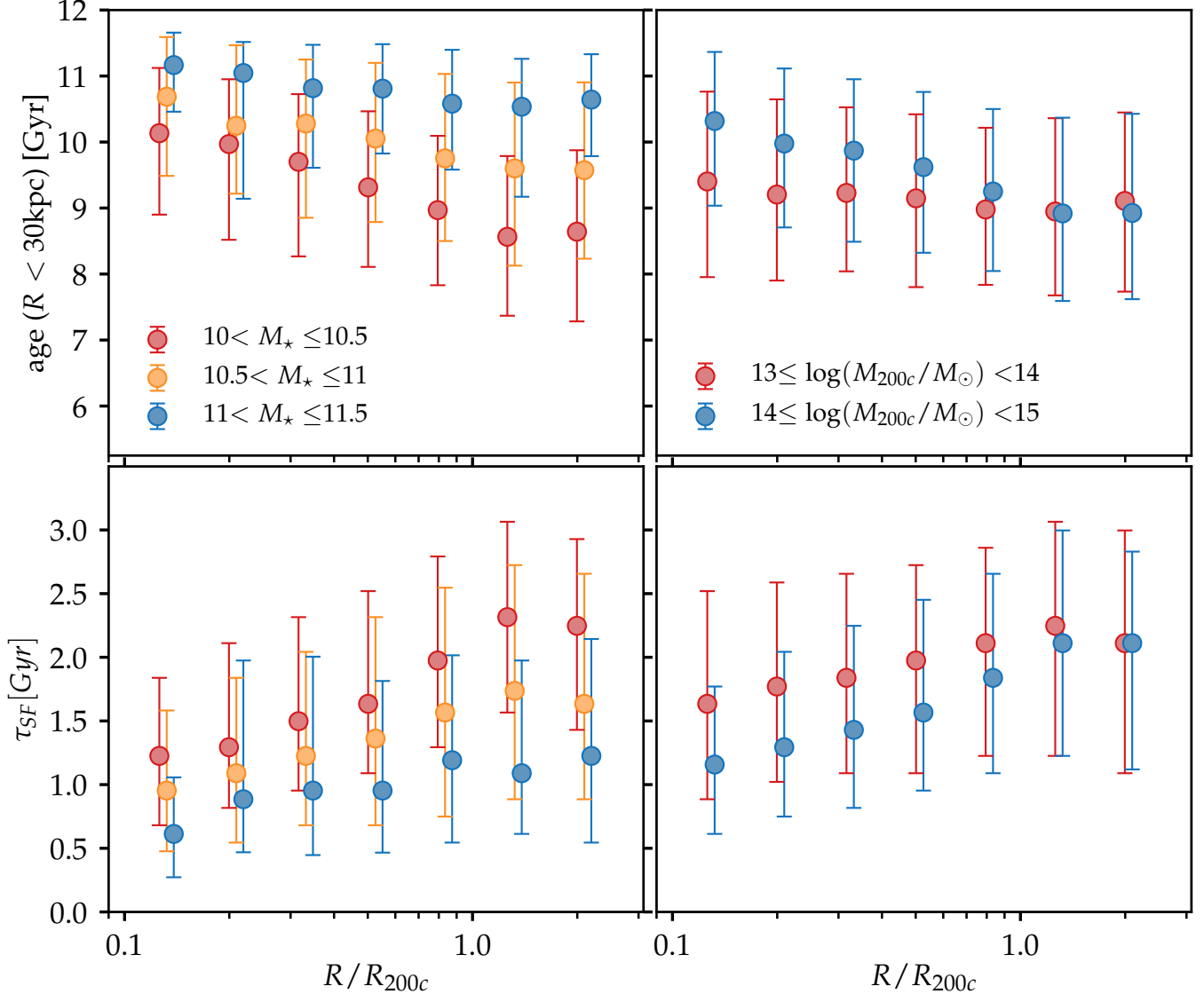


Figure 4. Mass-weighted stellar age and star formation timescales as a function of cluster-centric distances for quiescent satellite galaxies at $z=0$. We focus on galaxies in $\log(M_{200c,z=0}/M_{\odot}) > 14$ in the left panels, and galaxies with $10 \leq \log(M_{\star,R<30\text{kpc}}) < 11$ in the right panels.

final host halos at a later time than their direct infall counterparts. 3. For satellite galaxies that have been pre-processed, those in a more massive host halos at $z=0$ on average have a later accretion time into their final host halos. This 3rd point is not statistically strong though, and we need more data to verify it.

From the color-maps of star formation timescales and stellar ages, galaxies in more massive halos and those located closer to the central galaxies are formed earlier and cease star formation more abruptly. This is consistent with the coordinated assembly picture revealed by observational stellar population analysis: galaxies in the central regions of massive clusters have high $[\alpha/\text{Fe}]$ and old stellar ages. As a result, the most massive galaxies in the centers of the most massive dark matter halos will only get the chance to merge with those satellite galaxies that have old stellar ages, earlier quenching histories, and short star formation timescales. The assembled galaxies will imprint their stellar populations in the outskirts of massive galaxies, and this result can be examined by observational radial profiles of $[\alpha/\text{Fe}]$ and stellar ages.

3.2. Ages and Star Formation Histories

In Figure 2 we show the evolution of the $z=0$ quenched satellite galaxies in different environment. We focus on galaxies with $10 \leq \log(M_{\star,z=0}/M_{\odot}) < 11$. The top two panels show their accretion histories and evolution of sSFR in groups ($10^{13}M_{\odot} < M_{200c,z=0} \leq 10^{14}M_{\odot}$), and the bottom panels show the evolution in clusters ($10^{14}M_{\odot} < M_{200c,z=0} \leq 10^{15}M_{\odot}$). Galaxies are grouped by their relative cluster-centric distance at $z=0$ into 3 bins: $R \leq 0.5 \times R_{200c}$ (red), $0.5 \times R_{200c} < R \leq R_{200c}$ (orange) and $R_{200c} < R \leq 1.5 \times R_{200c}$ (blue). Squares mark the average time that galaxies are quenched. As shown in Figure 2, in both group and cluster environments, galaxies that are located closer to the primary galaxies have earlier accretion histories. Their sSFR falls faster and they are quenched earlier on average. Comparing galaxies with similar relative cluster-centric distances in group and cluster environments reveals that those in clusters have earlier accretion and quenching histories. Some galaxies are quenched even before they enter the R_{200c} of their final host dark matter ha-

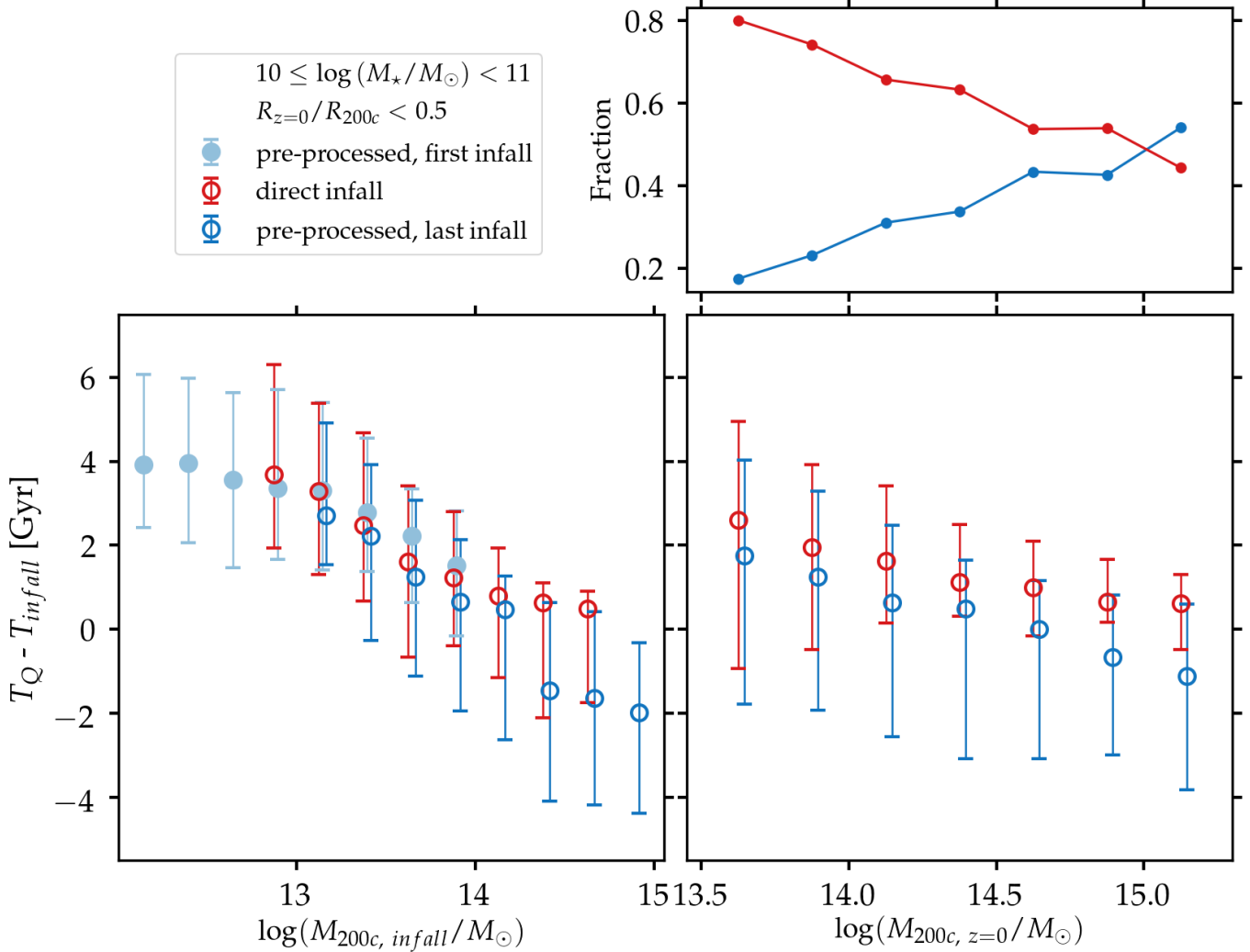


Figure 5. Top right: Fraction of satellite galaxies with $10 \leq (M_{*, R < 30 \text{kpc}, z=0}/M_{\odot}) < 11$ that have fallen into the final halo directly (red) and that have been group pre-processed (blue). Bottom panels show the time delay between infall and quenching time as a function of the halo mass at the infall time (left), and the halo mass at $z = 0$. Data are binned in 0.25 dex in halo mass, and only bins containing more than 25 galaxies are shown. Direct infall satellite galaxies experienced 0–3 Gyr delay between their infall and quenching time. Galaxies that had experienced group pre-processing in general have a 1–4 Gyr delay between their first infall and quenching time. For all galaxies the delay time is shorter in more massive host dark matter halos.

los, indicating that their gas has been stripped before entering their final host dark matter halos or pre-processed in smaller groups.

In Figure 3, we compare the $\tau_{SF}-M_{*}$ and stellar age- M_{*} scaling relations of the TNG300 quiescent galaxies with observed quiescent galaxies. Black dotted lines and the corresponding gray regions show observational results of stellar age and star formation timescale (50th, 16th and 84th percentiles) based on stacked SDSS early-type galaxies (ETGs) that are binned in stellar mass (Conroy et al. 2014). The stacked spectra are fit with the upgraded response functions. The star formation timescales are estimated using $[\alpha/\text{Fe}]$ of these stacked ETGs, and the conversion between $[\alpha/\text{Fe}]$ and star formation timescale based on a simple chemical evolution model in Thomas et al. 1999; Thomas et al. 2005: $[\alpha/\text{Fe}] \approx \frac{1}{5} - \frac{1}{6} \log(\Delta t/\text{Gyr})$. We examine how these scaling relations depend on cluster-centric distance (left panes, focusing on $\log(M_{200c}/M_{\odot}) > 14$) and halo mass (right panels, focusing on $R \leq 0.5 \times R_{200c}$) using TNG300 galaxies. The trends are calculated in 0.2 dex bins of $M_{*, R < 30 \text{kpc}}$. Only bins

including more than 25 galaxies are shown in the figure. The overall trends followed by TNG300 quiescent galaxies are in good agreement with observations. In both previous observations and this work, more massive galaxies are older and have short star formation timescales. More importantly, the TNG300 simulations predict strong variation in different environments: galaxies in the central regions and in more massive halos have shallower $\tau_{SF}-M_{*}$ and stellar age- M_{*} relations, indicating that in special environments, such as the central regions of galaxy clusters, even the relatively low mass galaxies have old stellar ages, and short star formation timescales in the past. This is consistent with the coordinated assembly picture.

Figure 4 shows the stellar ages and star formation timescales of quenched satellite galaxies as a function of relative cluster-centric distance in different environments. We focus on galaxies in $\log(M_{200c, z=0}/M_{\odot}) > 14$ in the left panels, and galaxies with $10 \leq \log(M_{*}/M_{\odot}) < 11$ in the right panels. The general trends are: satellite galaxies located further away from the primary galaxies are younger, and have longer star formation timescales in the past. From the left panels,

the dependence on cluster-centric distance is more robust for low mass galaxies. The left panels also predict that for galaxies in clusters with similar mass, the relation between stellar age and/or $[\alpha/\text{Fe}]$ and cluster-centric distance may have larger scatter towards the outskirts of galaxy clusters. From the right panels, galaxies in more massive dark matter halos are older and on average formed faster in the past, but this effect is only strong within R_{200c} .

3.3. Group Pre-processing

Previous work has highlighted the importance of group pre-processing on galaxy quenching histories (e.g. Fujita 2004; Balogh & McGee 2010; Wetzel et al. 2013; Bahé et al. 2019). In Figure 5, we look into the dependence on halo mass in detail, and examine whether group pre-processing plays a role in the coordinated assembly picture. We focus on satellite galaxies with $10 \leq \log(M_{*,z=0}/M_\odot) < 11$ that are located relatively close to the cluster centers ($\log(M_{200c,z=0}/M_\odot) > 14, R < 0.5 \times R_{200c}$). We identify satellite galaxies that fall into their $z = 0$ halos directly as central galaxies, and include them in the “direct infall” groups in Figure 5. The first time they are accreted into R_{200c} of their final host dark matter halos are marked as their infall times (red). Next, we identify those that were accreted onto their $z = 0$ halos as satellites, and look into the most recent time they fell into any dark matter halos with $\log(M_{200c,z=0}/M_\odot) > 12$ as central galaxies. We include these galaxies as “pre-processed” galaxies, and mark the time they are accreted as central galaxies as their first infall time (light blue), and the time they are accreted into their final host dark matter halos as the last infall time (blue). We note that one caveat comes from the uncertainty in merger scenarios where position-space halo finders may not successfully trace the separation of all subhalos.

The top right panel of Figure 5 shows the fraction of direct infall and group pre-processed galaxies as a function of their host dark matter halo mass at $z = 0$. In halos with $\log(M_{200c,z=0}/M_\odot) \sim 13.5$, 80% galaxies are accreted as central galaxies, and only $< 20\%$ have been pre-processed by a smaller halos. However, group pre-processing plays an increasingly important role in more massive galaxies. In the massive clusters with $\log(M_{200c,z=0}/M_\odot) \approx 15$, more than half the quenched galaxies have experienced group pre-processing.

In the bottom panels, we plot the delay between the quenching and infall times as a function of the halo mass at the infall time (left) and the halo mass at $z = 0$ (right). As shown in the bottom left panels, the time delay is shorter when galaxies are accreted into more massive dark matter halos. More importantly, the slopes of the relations between the time delay and the first infall halo mass are similar in both the “direct infall” and “pre-processed” cases, indicating that the quenching processes have already started since the first infall. If we only compare the time delay since the last infall, galaxies that have experienced group pre-processing have much shorter delay times than the direct infall galaxies, some of which are quenched even before they are accreted. This panel shows that group pre-processing is crucial in satellite quenching. The bottom right panel shows the time delay since their final accretion as a function of $z = 0$ halo mass. Galaxies that have been pre-processed have shorter time delays ($\approx -1 - 2$ Gyr) at all halo masses, while the direct infall galaxies are quenched 0–3 Gyr after they are accreted. In both cases galaxies are quenched faster in more massive groups and clusters. See Donnari et al. (2020) for additional in-depth characterization

of pre-processing with the IllustrisTNG simulations.

4. SUMMARY

In this Letter, we use TNG300 galaxies to explore the coordinated assembly picture (Gu et al. 2018), namely the idea that the ETGs in the central regions of galaxy clusters do not obey the $[\alpha/\text{Fe}]-M_*$ and age- M_* trends established by the general ETG sample, but instead follow much shallower relations. We try to understand whether the simulations show coordinated assembly and, if they do, what could be the underlying physical cause. We focus on quiescent satellite galaxies with $\log(M_{*,z=0}/M_\odot) \geq 10$ in massive halos ($M_{200c,z=0} \geq 10^{13} M_\odot$) from the TNG300 run. Our conclusions are summarized as follows:

- At $z = 0$, quenched satellite galaxies in the central regions of massive groups and clusters are accreted earlier, quenched earlier, have shorter star formation timescales and older stellar ages compared to their counterparts in other environments. This is consistent with observational results that galaxies in the central regions of massive clusters are old and α -enhanced.
- The star formation timescale (τ_{SF})- M_* and stellar age- M_* scaling relations followed by the TNG300 galaxies are in good agreement with observations. The slopes of these relations are much shallower in the central regions of massive dark matter halos, indicating that in this special environment even the low-mass ETGs have old stellar ages, and short star formation timescales.
- Both stellar ages and star formation timescales depend on cluster-centric distance. Galaxies in more massive dark matter halos are older and formed faster on average within R_{200c} . The dependence on cluster-centric distance is stronger for low mass galaxies.
- Group pre-processing is a crucial aspect in galaxy quenching, and plays an increasingly important role in more massive halos. Galaxies accreted into more massive groups and clusters are quenched faster, and the time delay is primarily determined by the halo mass of the first accretion.

To test the prediction of the environmental dependence in this work with observations, both halo mass and cluster-centric distance should be carefully measured from the observational side so that a robust comparison can be made. During the assembly of massive galaxies, the building blocks will imprint their stellar population signatures in the outskirts of these galaxies. Investigating the radial profiles of stellar population properties such as age and α -abundance in different environments, in both observations and simulations, will test the coordinated assembly picture.

This work made use of the COLOSSUS package (Diemer 2018). M.G. acknowledges support from the National Science Foundation Graduate Research Fellowship and the Henry Norris Russell Postdoctoral Fellowship. C.C. acknowledges support from NASA grant NNX15AK14G, NSF grant AST-1313280, and the Packard Foundation. FM acknowledges support through the Program “Rita Levi Montalcini” of the Italian MIUR. The computations in this paper were run on the Odyssey cluster supported by the FAS Division of Science,

Research Computing Group at Harvard University. The IllustrisTNG simulations used in this work have been run on the HazelHen Cray XC40-system at the High Performance Computing Center Stuttgart as part of project GCS-ILLU of the Gauss Centres for Supercomputing (GCS).

REFERENCES

- Abadi, M. G., Moore, B., & Bower, R. G. 1999, *MNRAS*, 308, 947 [1](#)
- Bahé, Y. M., Schaye, J., Barnes, D. J., et al. 2019, *MNRAS*, 485, 2287 [3.3](#)
- Balogh, M. L., & McGee, S. L. 2010, *MNRAS*, 402, L59 [3.3](#)
- Balogh, M. L., Navarro, J. F., & Morris, S. L. 2000, *The Astrophysical Journal*, 540, 113 [1](#)
- Conroy, C., Graves, G. J., & van Dokkum, P. G. 2014, *The Astrophysical Journal Letters*, 780, 33 [1](#), [3](#), [3.2](#)
- Cook, B. A., Conroy, C., Pillepich, A., Rodriguez-Gomez, V., & Hernquist, L. 2016, *ApJ*, 833, 158 [1](#)
- Davis, M., Efstathiou, G., Frenk, C. S., & White, S. D. M. 1985, *ApJ*, 292, 371 [2](#)
- Di Matteo, P., Pipino, A., Lehnert, M. D., Combes, F., & Semelin, B. 2009, *A&A*, 499, 427 [1](#)
- Diemer, B. 2018, *ApJS*, 239, 35 [4](#)
- Diemer, B., Sparre, M., Abramson, L. E., & Torrey, P. 2017, *ApJ*, 839, 26 [2](#)
- Dolag, K., Borgani, S., Murante, G., & Springel, V. 2009, *MNRAS*, 399, 497 [2](#)
- Donnari, M., Pillepich, A., Nelson, D., et al. 2019, *MNRAS*, 485, 4817 [2](#)
- Donnari, M., Pillepich, A., Joshi, G. D., et al. 2020, *arXiv*, 2008.00005 [1](#), [3.3](#)
- Farouki, R., & Shapiro, S. L. 1981, *ApJ*, 243, 32 [1](#)
- Fujita, Y. 2004, *PASJ*, 56, 29 [3.3](#)
- Genel, S., Vogelsberger, M., Springel, V., et al. 2014, *MNRAS*, 445, 175 [2](#)
- Genel, S., Nelson, D., Pillepich, A., et al. 2018, *MNRAS*, 474, 3976 [2](#)
- Gu, M., Conroy, C., & Brammer, G. 2018, *The Astrophysical Journal Letters*, 862, L18 [1](#), [4](#)
- Gunn, J. E., & Gott, III, J. R. 1972, *ApJ*, 176, 1 [1](#)
- Larson, R. B., Tinsley, B. M., & Caldwell, C. N. 1980, *ApJ*, 237, 692 [1](#)
- Marinacci, F., Vogelsberger, M., Pakmor, R., et al. 2018, *MNRAS*, 480, 5113 [1](#), [2](#)
- Moore, B., Katz, N., Lake, G., Dressler, A., & Oemler, A. 1996, *Nature*, 379, 613 [1](#)
- Naab, T., Johansson, P. H., & Ostriker, J. P. 2009, *ApJ*, 699, L178 [1](#)
- Naiman, J. P., Pillepich, A., Springel, V., et al. 2018, *MNRAS*, 477, 1206 [1](#), [2](#)
- Nelson, D., Kauffmann, G., Pillepich, A., et al. 2018, *Monthly Notices of the Royal Astronomical Society*, 477, 450 [1](#), [2](#)
- Nelson, D., Pillepich, A., Springel, V., et al. 2019a, *MNRAS*, 490, 3234 [1](#), [2](#)
- Nelson, D., Springel, V., Pillepich, A., et al. 2019b, *Computational Astrophysics and Cosmology*, 6, 2 [1](#), [2](#)
- Oser, L., Naab, T., Ostriker, J. P., & Johansson, P. H. 2012, *ApJ*, 744, 63 [1](#)
- Oser, L., Ostriker, J. P., Naab, T., Johansson, P. H., & Burkert, A. 2010, *ApJ*, 725, 2312 [1](#)
- Patel, S. G., van Dokkum, P. G., Franx, M., et al. 2013, *ApJ*, 766, 15 [1](#)
- Peng, Y.-j., Lilly, S. J., Renzini, A., & Carollo, M. 2012, *ApJ*, 757, 4 [1](#)
- Peng, Y.-j., Lilly, S. J., Kovac, K., et al. 2010, *The Astrophysical Journal Letters*, 721, 193 [1](#)
- Pillepich, A., Nelson, D., Hernquist, L., et al. 2018, *Monthly Notices of the Royal Astronomical Society*, 475, 648 [1](#), [2](#)
- Pillepich, A., Nelson, D., Springel, V., et al. 2019, *MNRAS*, 490, 3196 [1](#), [2](#)
- Planck Collaboration, Ade, P. A. R., Aghanim, N., et al. 2016, *A&A*, 594, A13 [2](#)
- Rhee, J., Smith, R., Choi, H., et al. 2017, *ApJ*, 843, 128 [3.1](#)
- Rodriguez-Gomez, V., Genel, S., Vogelsberger, M., et al. 2015, *Monthly Notices of the Royal Astronomical Society*, 449, 49 [2](#)
- Rodriguez-Gomez, V., Pillepich, A., Sales, L. V., et al. 2016, *MNRAS*, 458, 2371 [2](#)
- Rodriguez-Gomez, V., Snyder, G. F., Lotz, J. M., et al. 2019, *MNRAS*, 483, 4140 [2](#)
- Springel, V., White, S. D. M., Tormen, G., & Kauffmann, G. 2001, *MNRAS*, 328, 726 [2](#)
- Springel, V., Pakmor, R., Pillepich, A., et al. 2018, *MNRAS*, 475, 676 [1](#), [2](#)
- Thomas, D., Greggio, L., & Bender, R. 1999, *Monthly Notices of the Royal Astronomical Society*, 302, 537 [3.2](#)
- Thomas, D., Maraston, C., Bender, R., & Mendes de Oliveira, C. 2005, *ApJ*, 621, 673 [1](#), [3.2](#)
- Trager, S. C., Faber, S. M., Worthey, G., & González, J. J. 2000, *The Astronomical Journal*, 119, 1645 [1](#)
- van Dokkum, P. G., Whitaker, K. E., Brammer, G., et al. 2010, *ApJ*, 709, 1018 [1](#)
- Vogelsberger, M., Genel, S., Springel, V., et al. 2014a, *MNRAS*, 444, 1518 [2](#)
- . 2014b, *Nature*, 509, 177 [2](#)
- Wetzel, A. R., Tinker, J. L., Conroy, C., & Bosch, F. C. v. d. 2014, *Monthly Notices of the Royal Astronomical Society*, 439, 2687 [1](#)
- Wetzel, A. R., Tinker, J. L., Conroy, C., & van den Bosch, F. C. 2013, *Monthly Notices of the Royal Astronomical Society*, 432, 336 [1](#), [3.3](#)